



Examination of experimental variability in HFFB testing of a tall building under multi-directional winds



Wei Cui, Luca Caracoglia*

Department of Civil and Environmental Engineering, Northeastern University, Boston, MA 02115, USA

ARTICLE INFO

Keywords:

Tall building aerodynamics
Wind tunnel experiments
Power spectral density
Experimental errors

ABSTRACT

Examination of wind loading uncertainty is necessary for structural fragility analysis of tall buildings in the context of performance-based wind engineering. One of the sources of uncertainty is represented by random experimental error, which may occur during a standard test in wind tunnel, such as the high frequency force balance (HFFB) test. Few examples of systematic experimental error analysis are available. This study examines a series of experiments on a model of a standard benchmark building under simulated turbulent flow. HFFB experiments were conducted in the Northeastern University's small-scale wind tunnel. Three model equations are proposed to represent the power spectral density (PSD) functions of the above three forces in the frequency domain.

Furthermore, effects of experimental errors are incorporated by allowing the parameters in each function to vary randomly. Variability is evaluated by considering the second-order statistical moments of the parameters (standard deviations and correlations). At last, this paper introduces a data-driven Monte-Carlo approach to reconstruct the generalized PSD of the wind loading through model equations. Experimental variability is accounted for by exploiting information on the probability distributions of the model parameters. Verification of the reconstructed PSD functions against experiments suggests that the Monte-Carlo approach can effectively generate synthetic PSD curves.

1. Introduction

1.1. Performance-based design in wind engineering: recent studies

High winds are among the most destructive natural hazards besides earthquakes. Strong winds can cause severe damage to properties and loss of life. The severity of wind hazards, their perceived threat and the recurrence of wind-induced damage have motivated comprehensive research activities aiming to more accurately assess structural safety under extreme wind conditions. Unlike the more established performance-based criteria in seismic engineering, a general consensus on a standardized approach for performance-based wind-resistant design has not been achieved yet. Pioneering work by Ellingwood et al. (2004) and Ellingwood and Tekie (1999) proposed a rigorous probabilistic analysis of wind loads and structural performance uncertainties to examine wind effects on low-rise wood structures. Along the same line of study, Chock et al. (1998) attempted to establish wind-resistant design criteria, which are compatible with basic concepts of performance-based seismic design. Van de Lindt and Dao (2009) advanced the concept of

performance-based wind engineering for wood-frame buildings through the derivation of structural fragility curves to meet various owner/user performance expectations, which include occupant comfort, continued occupancy, life safety and structural integrity. In the case of tall buildings, Pozzuoli et al. (2013) presented an operational method, based on wind tunnel measurements, to evaluate the discomfort risk for occupants, which considers various wind speeds and directions and combines the effects of both the along-wind and cross-wind loads. Multi-directional wind effects are on occasion considered as an integral part of the design process [e.g., (Jain et al., 2001)].

Several researchers have also recently examined a number of optimization methods to expand into practice the concepts of performance-based engineering (PBE) to tall buildings under wind loads. Recent advances in high-performance computing have enabled massive calculations, needed for uncertainty. For example, Huang et al. (2012) proposed a structural optimization procedure to account for uncertainties in the wind loads by decoupling lateral drift and acceleration. Spence and Kareem (2014) examined a probabilistic optimization strategy for PBE and uncertainty simulations of linear building systems, driven by

* Corresponding author. Department of Civil and Environmental Engineering, Northeastern University, 400 Snell Engineering Center, 360 Huntington Avenue, Boston, MA 02115, USA.
E-mail address: lucac@coe.neu.edu (L. Caracoglia).

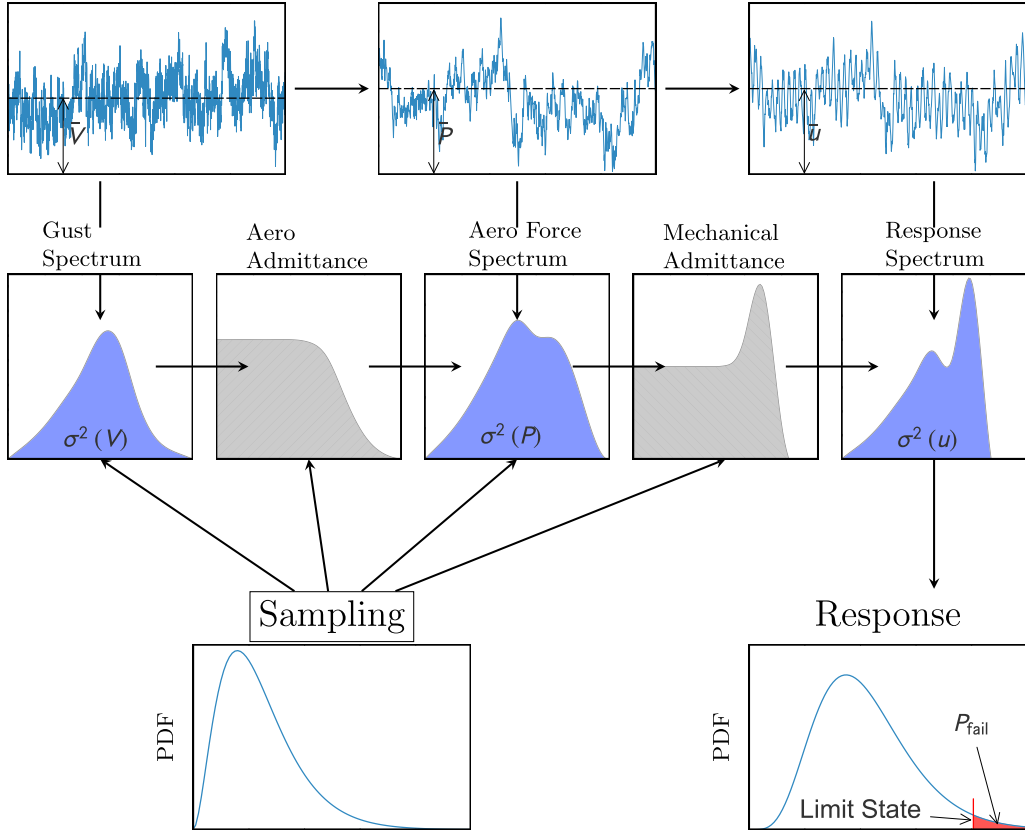


Fig. 1. Davenport Chain and its relationship to wind-induced response and uncertainty analysis.

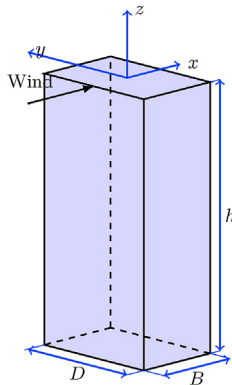


Fig. 2. Schematic view of the CAARC building.

experimentally determined stochastic wind loads; this approach has been later adapted to occupant comfort and serviceability limit states by [Bernardini et al. \(2014\)](#). This is only a brief review of the main research contributions in this emerging research field, which still deserves careful attention and further investigations.

1.2. Research motivation in the context of wind load analysis on tall buildings

The state-of-the-art structural performance analysis method against wind loads is based on three-dimensional models of the wind load ([Piccardo and Solari, 2000, 1998a; Chen and Kareem, 2005a, 2005b; Tse et al., 2009b](#)). The current wind tunnel procedures for estimating wind loading on a tall building are critically examined in this paper. One of the sources of uncertainty is represented by random

experimental error, which may occur during a standard test in wind tunnel, such as the high frequency force balance (HFFB) test. This test is routinely employed by researchers and practitioners to estimate wind loads and predict the response of the building at full scale. Despite the several decades of research in the field of building aerodynamics, few examples of experimental error analysis are available. This study proposes an experimental approach that incorporates information on the experimental variability in the estimation of the wind loads. A series of experiments are conducted on a model of the CAARC (Commonwealth Advisory Aeronautical Research Council) benchmark building under simulated turbulent flow for various incoming wind directions. This is also the first step towards the implementation of a comprehensive operational framework for performance-based wind-resistant design of tall buildings, which simultaneously accounts for wind directionality and experimental variability in the estimation of structural fragility.

2. Background theory

2.1. Davenport's wind loading chain

The foundation of wind engineering analysis was established by Alan Davenport's Ph.D. dissertation ([Davenport, 1961](#)). Wind-induced structural response can be determined in the frequency domain through the combination of local wind climatology, topography, structural aerodynamic and structural dynamic properties. The process is summarized in Fig. 1, reproduced from [Davenport \(1961\)](#). Nowadays, this approach is designated as "Davenport Chain" ([Isyumov, 2012](#)).

Since the original formulation of "Davenport Chain", numerous contributions have been made by the research community to investigate wind loading, aerodynamics and structural response in each steps and try to accurate evaluation structural performance under strong wind.

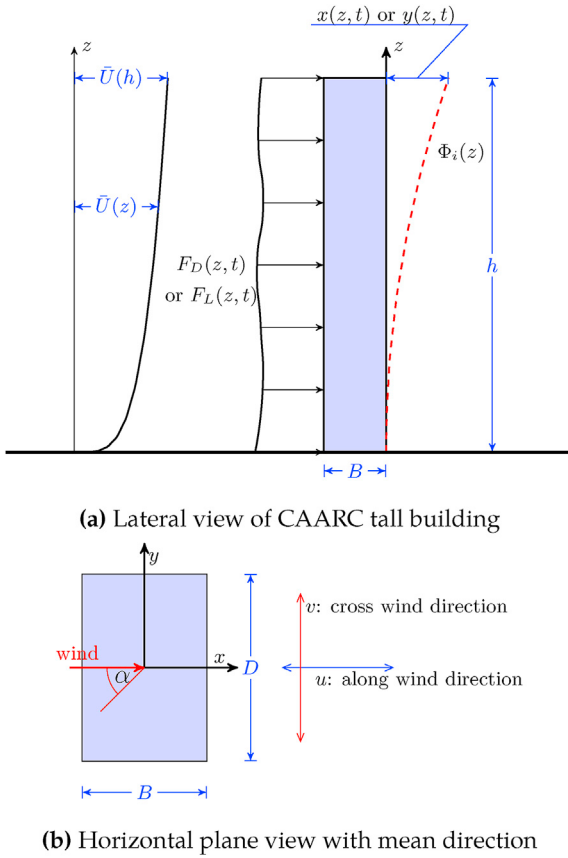


Fig. 3. Schematic of tall building aerodynamics and wind-load directionality (α is the relative mean-wind direction angle).

2.2. Quasi-static wind-induced response analysis method

The standard frequency domain random vibration analysis has traditionally been utilized to estimate the wind-induced loading and dynamic response of tall buildings (Davenport, 1988, 1971; Piccardo and Solari, 1998b). For serviceability limit states, usually predominant in the wind-resistant design of tall buildings, a linear elastic structural model is normally accepted (Davenport, 1988).

The building model in this study reflects the properties of the CAARC benchmark building (Melbourne, (1980)). This building has been used as a reference model for the comparison among several experimental methods and analysis techniques. Fig. 2 shows a schematic view of the CAARC building with an indication of the main dimensions of the structure (depth D , width B , height h).

This building is modeled as a slender prismatic cantilever structure with a rectangular floor-plan section. The structure is symmetrical to both (strong and weak) axes of lateral bending. The mean wind direction with $\alpha = 0$ coincides with the direction x in Fig. 3(b). Applying the quasi-static theory (Davenport, 1971; Kareem, 1982), the PSD of the generalized turbulence-induced (buffeting) dynamic force can be determined. As an example, Eq. (1) presents the formula of the wind loading in the along-wind direction.

$$S_{Q,Q_x}(n) = \iint_h C_D^2 \rho^2 D^2 \Phi_x(z_1) \Phi_x(z_2) \bar{U}(z_1) \bar{U}(z_2) S_{uu}(n, z_1, z_2) dz_1 dz_2 \quad (1)$$

In the previous equation ρ is the air density, $\Phi_x(z)$ is the mode-shape function in along-wind direction; $\bar{U}(z)$ is the mean wind velocity at height z ; D is a reference width of the building section (Fig. 3(b)) and C_D is the drag coefficient.

The frequency domain theory allows to calculate the PSD of the

building response from the PSD of the generalized dynamic force. As an example, Eq. (2) presents the PSD of the along-wind response in the x direction between any two point at height z_1 and z_2 :

$$S_{xx}(z_1, z_2, n) = \frac{\Phi_x(z_1) \Phi_x(z_2) S_{Q_x Q_x}}{16\pi^2 M_{g,x}^2 [(n_{0,x}^2 - n^2)^2 + [2nn_{0,x}(\zeta_{s,x} + \zeta_{a,x})]^2]} \quad (2)$$

In the previous equation $n_{0,x}$ is the fundamental natural frequency for lateral bending in the x direction; $M_{g,x}$ is the generalized mass derived from the mode shape function $\Phi_x(z)$; $\zeta_{s,x}$, $\zeta_{a,x}$ respectively are structural damping and aerodynamic damping evaluated for the x direction. The analysis procedure is similar for cross-wind response, which is omitted here for the sake of brevity but may be found, for example, in other references (Piccardo and Solari, 1998a; Dyrbye and Hansen, 1997).

2.3. Monte-Carlo sampling for wind loading variability analysis and uncertainty propagation

The Monte-Carlo sampling method is predominantly employed for uncertainty simulation, needed by PBE (Smith and Caracoglia, 2011; Seo and Caracoglia, 2012; Cui and Caracoglia, 2015). The probability of structural “failure” P_{fail} (i.e., exceedance of a pre-selected design threshold level) can be conveniently computed as follows:

$$P_{fail} \approx \frac{1}{N} \sum_{i=1}^N \delta(V_i) \quad (3)$$

with $\delta(V_i)$ denoting an indicator function which depends on a set of uncertain engineering demand parameters V_i evaluated over the sample N . This concept is briefly explained in the “sampling step” of Fig. 1; $\delta(V_i)$ is defined as

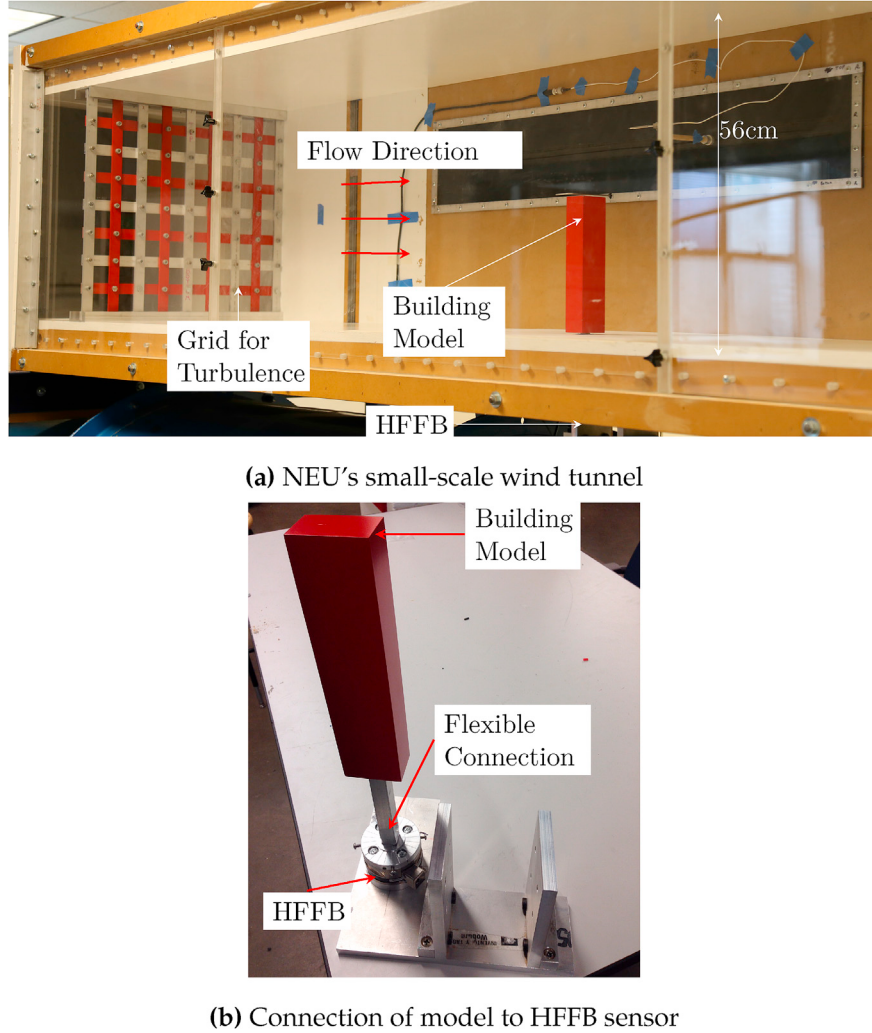
$$\delta = \begin{cases} 1 & \text{structural response exceeds limit state threshold} \\ 0 & \text{otherwise} \end{cases} \quad (4)$$

The P_{fail} can therefore be found by repeating the random analysis N times.

As illustrated in Fig. 1 and in Eq. (2), several parameters are involved in each step of the Davenport Chain, such as mean wind velocity $\bar{U}(z)$ and turbulence intensity of the turbulence spectrum, drag coefficients C_D , lift coefficients C_L with their derivatives with respect to α , etc. The presence of several uncertain parameters makes the estimation of the failure domain very convoluted (Smith and Caracoglia, 2011; Seo and Caracoglia, 2012; Cui and Caracoglia, 2015). Furthermore, implementation of other alternative methods for aeroelastic uncertainty propagation, such as stochastic calculus (Caracoglia, 2014), are not always recommended.

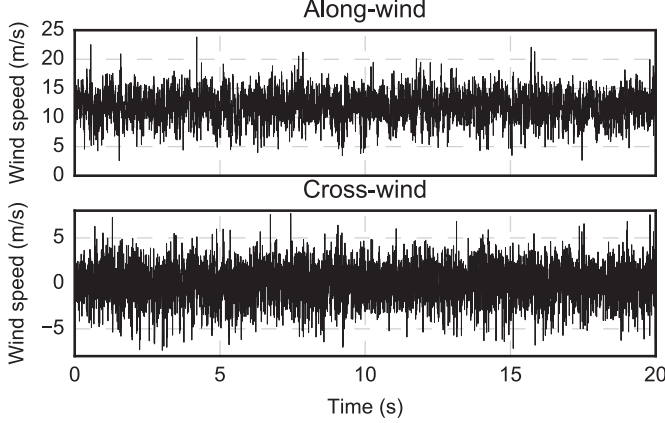
2.4. Wind tunnel experimental method to evaluate wind loads on tall buildings

The HFFB technique, which has been briefly outlined in the introduction of this paper, has been usually preferred by researchers and practitioners (Davenport and Tschanz, 1981; Kareem and Cermak, 1978; Tschanz and Davenport, 1983; Reinhold and Kareem, 1986; Boggs and Peterka, 1989) to estimate wind loads. The wind tunnel experiment is carried out by exposing a tall building model to a boundary layer flow, which replicates the full-scale atmospheric conditions. Measurements of the base forces enable the direct derivation of generalized loads, needed to estimate the structural response. This process is, however, not always straightforward since it involves several assumptions, such as uncoupled lateral mode shapes linearly varying with height. Several methods for circumventing this limitation are available [e.g., (Holmes, 1987)]. For



(b) Connection of model to HFFB sensor

Fig. 4. Experimental setup in NEU's wind tunnel.

Fig. 5. Horizontal wind speed time series in the along-wind ($\bar{U} + u$) and cross-wind (v) directions ($\bar{U} = 11.8\text{m/s}$).

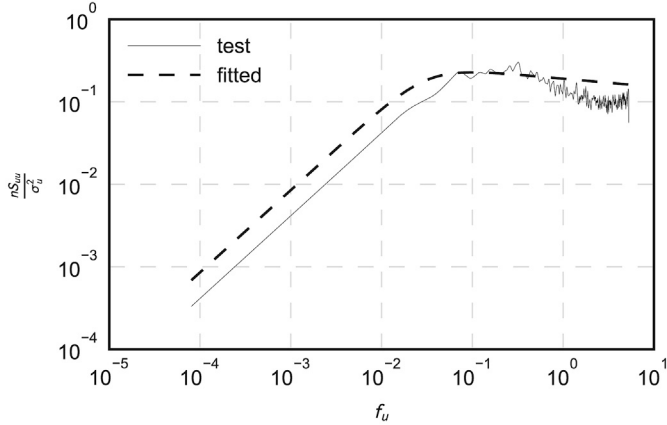
instance, the mode shape can be corrected according to an equivalent static wind load (Zhou et al., 2002). As an alternative, Chen and Kareem (2005c) examined a framework to determine the distribution of spatio-temporal fluctuations of the wind loads on the tall building, which eliminates the need for mode shape corrections.

As an substitute to wind tunnel methods, numerical methods have

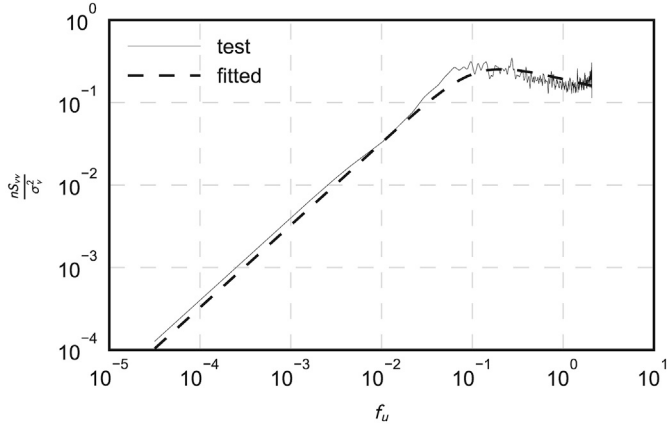
been used to study aerodynamic loads. Several studies [e.g., (Corrigan et al., 2011; Huang et al., 2007)] have considered computational fluid dynamics (CFD) to estimate wind loads; recent results confirm the accuracy and efficiency of the CFD method [e.g., (Elshaer et al., 2016)], also for structural optimization Lee et al. (2012). Nevertheless, a PBE-oriented analysis requires the examination of several uncertainty sources. Among these sources, uncertainty in aerodynamic force estimation can be identified from a wind tunnel test (Seo and Caracoglia, 2012), less efficiently from a field investigation [e.g., (Caracoglia et al., 2008)] and from CFD simulations.

In accordance with the fundamentals of Davenport Chain and wind tunnel testing methods, most researchers independently identify every parameter in each step of the chain. Nevertheless, identification of numerous parameters needs a large data set from various wind tunnel experiments, which are necessary to also capture vortex shedding. These parameters are usually not readily accessible. Moreover, in the presence of unconventional mode shapes and multi-modal response, the computing time of the generalized modal forces, such as S_{Q,Q_x} in Eq. (1), will increase exponentially with the number of modes.

For these two reasons, the implementation of PBE in wind engineering is still challenging. In order to overcome the limitations, a wind tunnel test procedure followed by an *a-posteriori* data analysis method is proposed in this paper as the first module towards the implementation of a comprehensive framework for efficient uncertainty analysis of tall building aerodynamics.



(a) Along-wind turbulence



(b) Cross-wind turbulence

Fig. 6. Experimental turbulence spectra measured in NEU's wind tunnel as a function of dimensionless frequency $f_u = nL_{tx}/\bar{U}$: example.

3. Description of the experimental setup and testing procedure

3.1. Northeastern University's small-scale wind tunnel: analysis of the HFFB setup and examination of its adequacy

Wind tunnel tests were carried in the Northeastern University's (NEU's) small-scale closed-circuit wind tunnel, shown in Fig. 4(a). Dimensions of the test chamber are 560×560 mm; the maximum flow speed in the test chamber is about 20 m/s. As a first approximation of a boundary-layer wind simulation for high-rise buildings, turbulence is generated by a grid. The width of each rectangular-section bar of the grid is 2 cm; the depth is less than 0.5 cm and the center-to-center distance between each bar is 4 cm in both vertical and horizontal directions. The solidity ratio of the grid is 0.333. Along-wind turbulence intensity at the location of the model (1.32 m downstream from the grid) is approximately 18.6% (Fig. 4(a)). The length scale of turbulence is approximately 5 cm. This value was estimated from the temporal auto-correlation function of the along-wind horizontal turbulence component, measured at 36 cm from the base of the chamber and is compatible with the size of the grid used for homogeneous turbulence generation. The building model represents, at a 1:750 scale, the characteristics of the CAARC standard building (Melbourne, 1980). Model dimensions are as follows: rectangular base of width $D = 71$ mm, depth $B = 47.3$ mm and height $h = 284$ mm; the ratio of the sides is 1:1.5:6. Consequently, wind tunnel blockage is still small (4%) and no post-processing of the measured forces was considered to adjust for this effect. In order to avoid resonant effects in the HFFB setup at low to moderate frequencies, the mass of the model

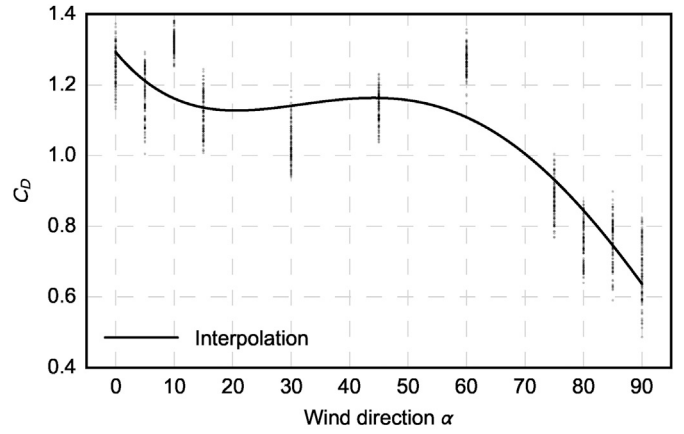
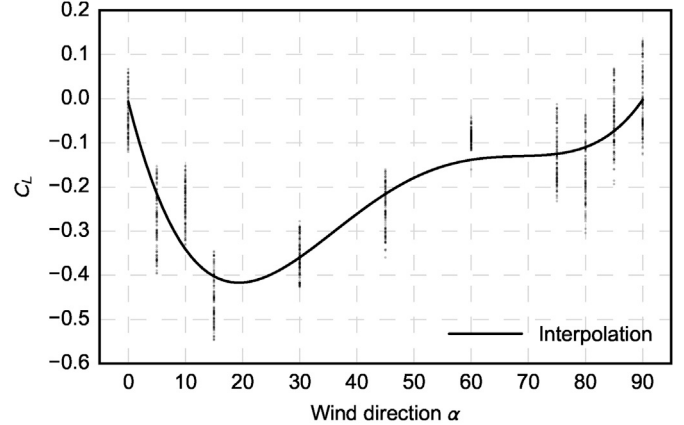
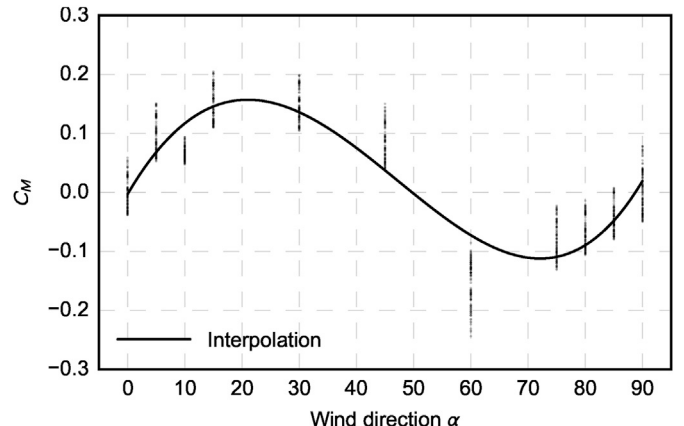
(a) C_D (b) C_L (c) C_M

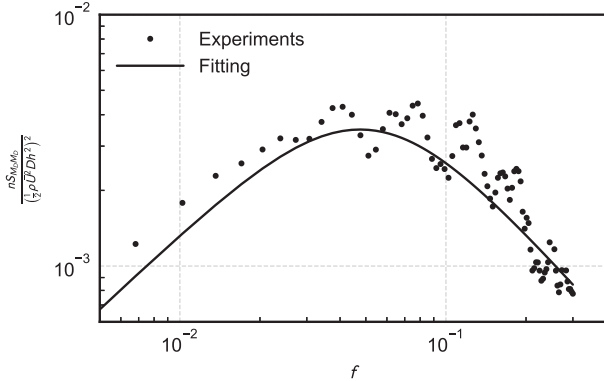
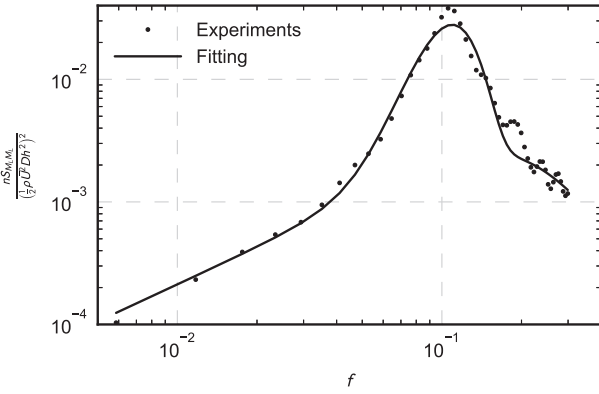
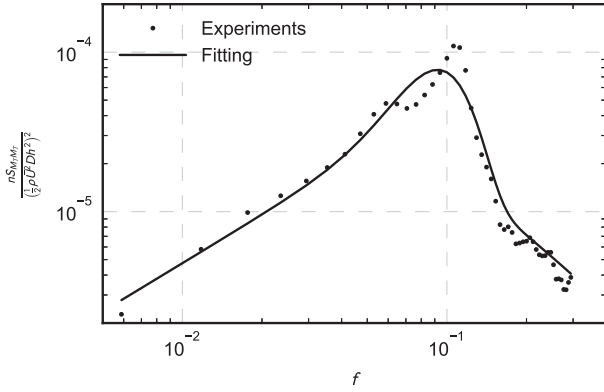
Fig. 7. Variation of CAARC static aerodynamic coefficients with mean wind direction α [deg].

and connection detail were designed to be as small as possible. The mass of the building, made of hard hollow plastic, is approximately equal to 300 g (Fig. 4(a)). The model was connected to the HFFB sensor through a hollow square aluminum tube, whose dimensions are $19 \times 19 \times 6.4$ mm, see Fig. 4(b). The base force sensor (HFFB) is an ATI Industrial Automation six-axis Gamma-type force balance; it was mounted on a rigid aluminum plate and placed beneath the chamber to acquire the force data, see Fig. 4(a).

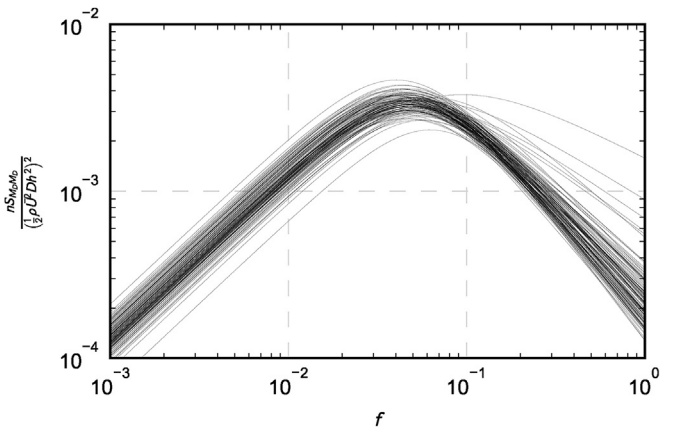
For the purpose of illustrating the applicability of the proposed

Table 1Parameter values for C_D , C_L and C_M in Eq. (7) (α expressed in degrees).

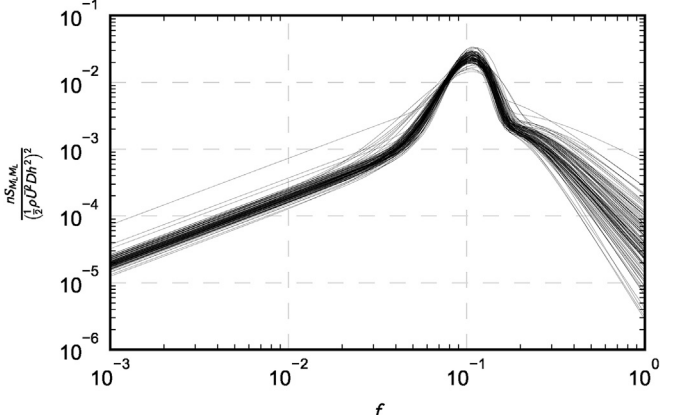
| a_0 | a_1 | b_1 | a_2 | b_2 | w |
|-------|--------|---------|---------|---------|---------|
| C_D | 1.0465 | -0.0153 | 0.1565 | 0.1926 | 0.0293 |
| C_L | 0.2471 | -0.0158 | -0.7426 | -0.2809 | -0.1392 |
| C_M | 0.0223 | 0.0754 | 0.0842 | -0.0710 | -0.0020 |

Fig. 8. PSD of along-wind base bending moment and fitting results at $\alpha = 0^\circ$.Fig. 9. PSD of cross-wind base bending moment and fitting results at $\alpha = 0^\circ$.Fig. 10. PSD of base torque and fitting results at $\alpha = 0^\circ$.

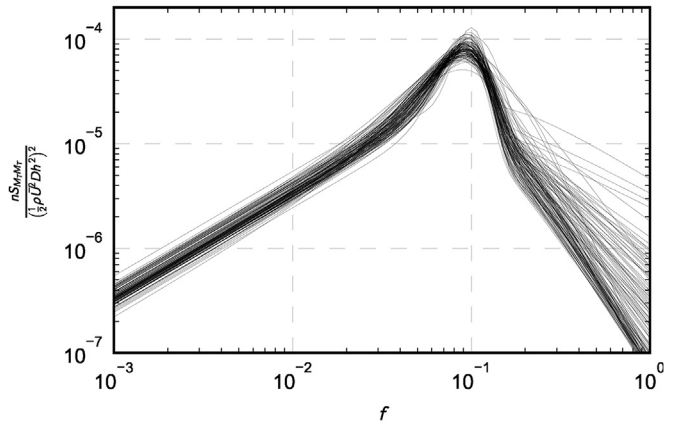
method, preliminary tests were carried out at mean-wind incident angle $\alpha = \{0^\circ, 90^\circ\}$, mean flow speed \bar{U} variable between 8 m/s and 10 m/s and uniform turbulence. Unfortunately, boundary layer flow cannot be easily simulated in this small facility. Therefore, quantitative differences are anticipated between the measured base forces and the references values



(a) Along-wind base bending moment



(b) Cross-wind base bending moment



(c) Base torque

Fig. 11. CAARC building model: repeated realizations (variability) of the experimental wind force PSD for mean wind direction $\alpha = 0^\circ$.

indicated by Melbourne (1980), Saunders and Melbourne (1975) and derived from several other laboratories. Preliminary comparison of the results were presented in Cui and Caracoglia (2016). The results are not reported in this study for the sake of brevity; they suggest some small quantitative differences between the HFFB base force and moment spectra, measured at NEU, and the reference spectra published by Saunders and Melbourne (1975). In spite of the differences, the

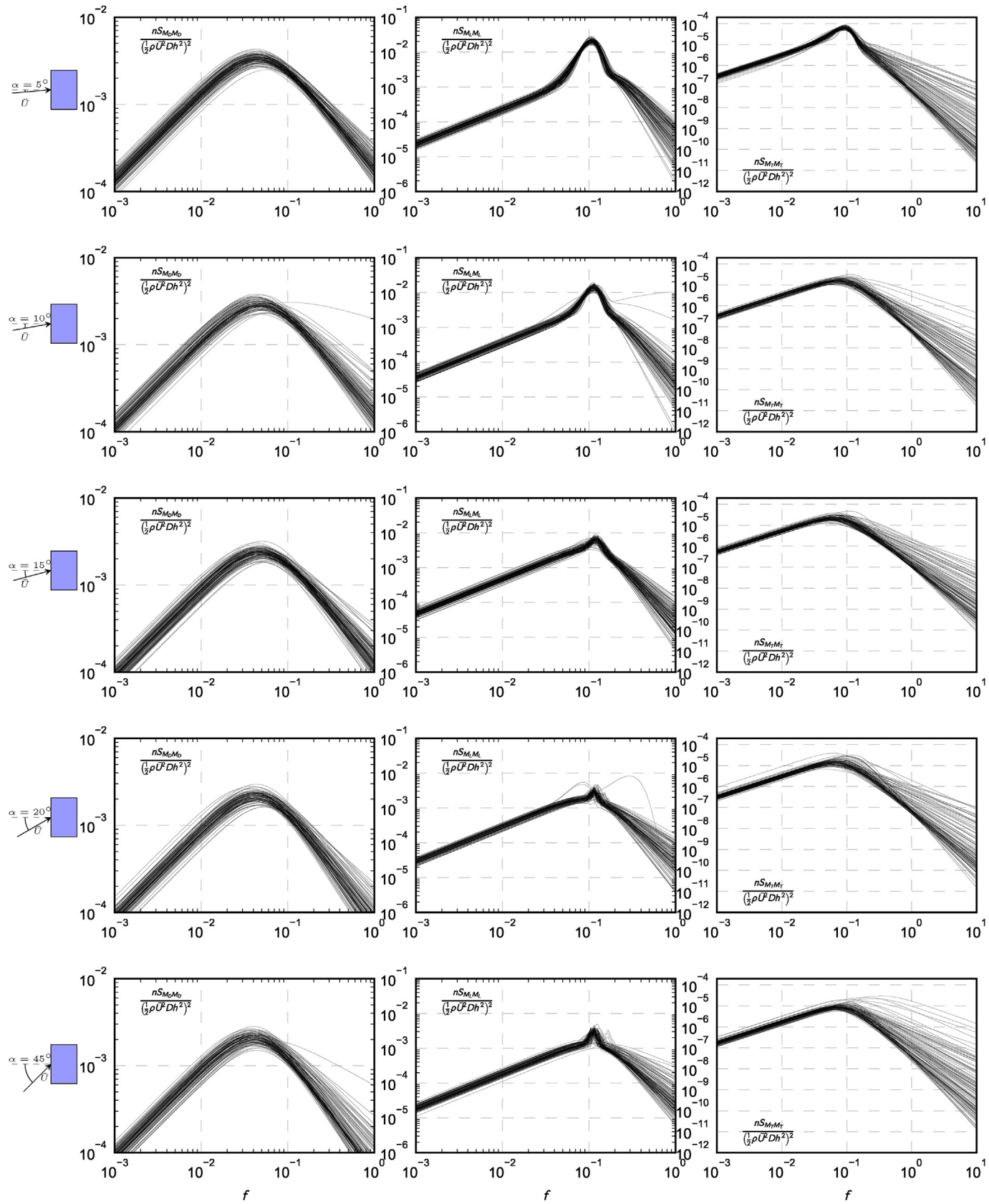


Fig. 12. CAARC building model: experimental curves of the generalized wind force PSD for mean wind directions $\alpha = 5^\circ, 10^\circ, 15^\circ, 30^\circ, 45^\circ$.

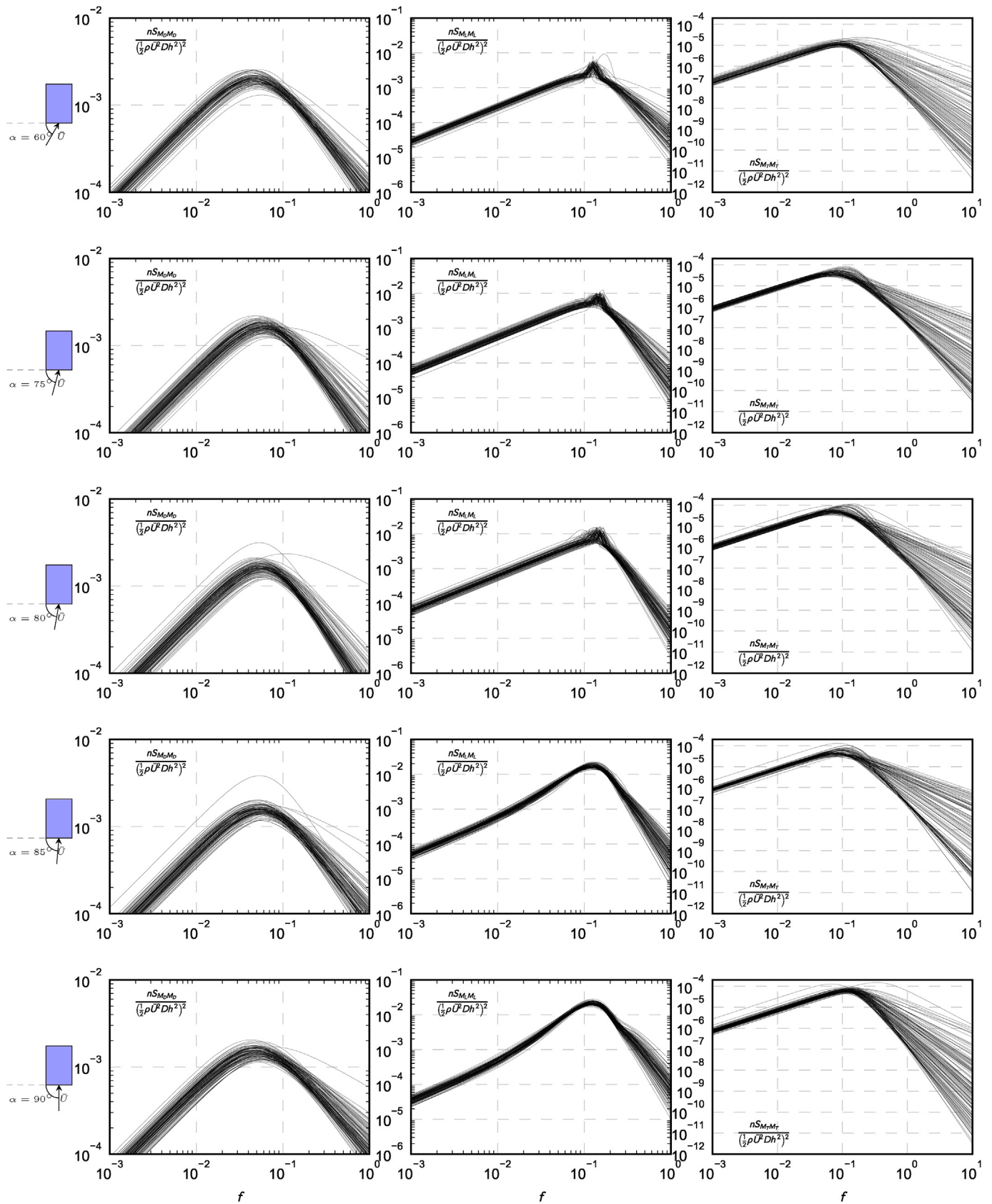


Fig. 13. CAARC building model: experimental curves of the generalized wind force PSD for mean wind directions $\alpha = 60^\circ, 75^\circ, 80^\circ, 85^\circ, 90^\circ$.

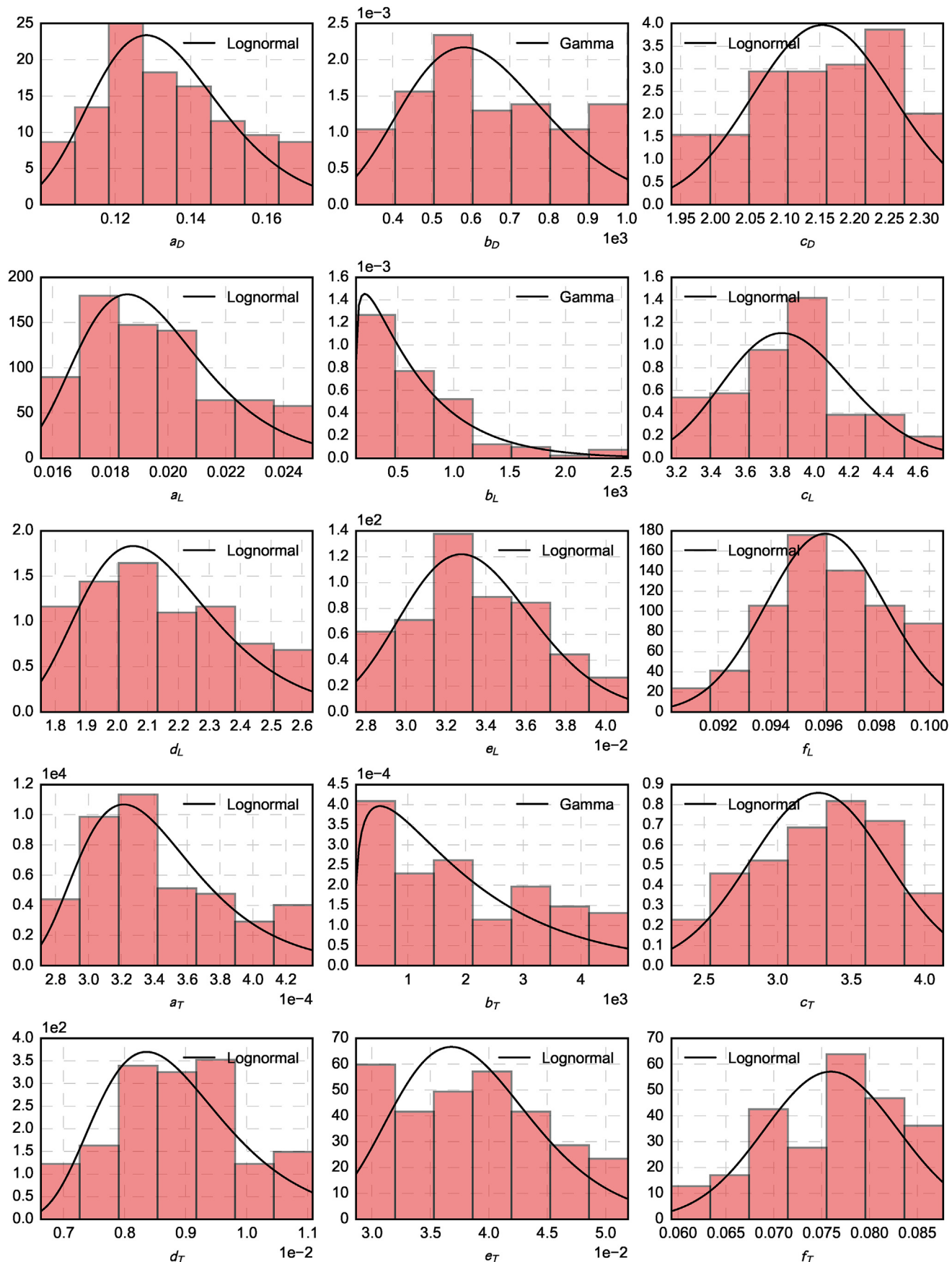


Fig. 14. CAARC building model: empirical histograms of the model curve parameters in Eqs. (9)–(11)), found by fitting the experimental curves of the generalized wind force PSD at $\alpha = 0^\circ$.

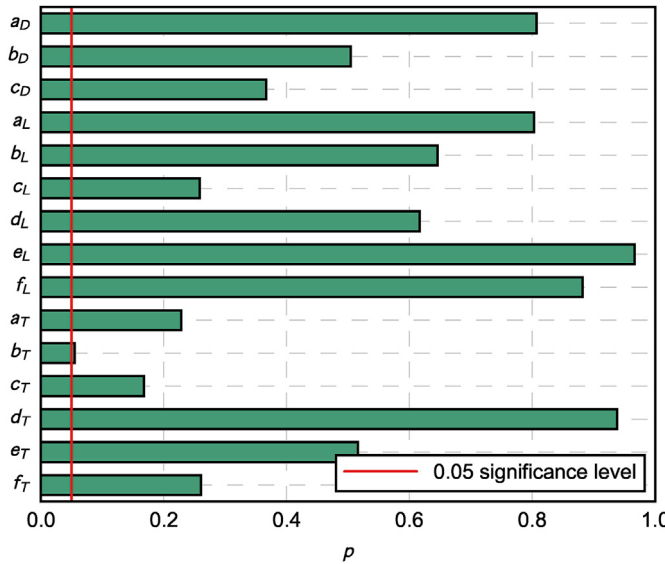


Fig. 15. Results of the goodness-of-fit hypothesis tests (p value) for the parameters of the CAARC building model at $\alpha = 0^\circ$.

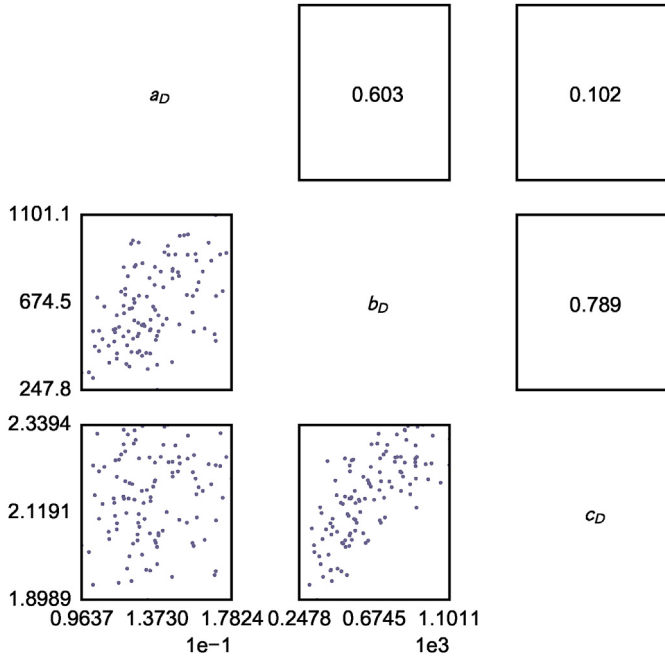


Fig. 16. Coefficients of correlation among the parameters in Eq. (9) for the CAARC building model.

preliminary study (Cui and Caracoglia, 2016) indicated that the setup is adequate for the purpose of measurement and comparison of base forces due to turbulent wind loads. Moreover, such differences are acceptable in the context of the experimental analysis and identification procedure discussed herein, since the primary purpose of the investigation is the examination of the random experimental error.

3.2. Wind flow characteristics in the NEU's wind tunnel

As discussed in the previous sub-section, a homogeneous-turbulence wind flow can exclusively be generated in NEU's wind tunnel. The turbulence intensity is determined by flow measurements using the grid turbulence "generator". The mean wind speed and turbulence intensity are approximately constant along wind tunnel height. The latter was

measured as approximately 18.6% [i.e., larger than 14%, indicated by Melbourne (1980)] independent of mean wind speed.

Turbulent flow speed was measured by DANTEC dual-sensor gold-plated hot-wire probes (model P9055P0611); the cross-wire was appropriately oriented to simultaneously record wind speed time series in the two horizontal directions, along-wind or u (i.e., along the longitudinal axis of the test chamber) and cross-wind or v . Fig. 5 illustrates an example of wind speed record in the two directions, sampled at 1 kHz, when mean flow speed in the chamber is $\bar{U} = 11.8$ m/s.

The PSD of the turbulence can be subsequently estimated from the time series using Welch's method. The two PSD experimental curves are shown in Fig. 6. The PSD of turbulence S_{uu} is represented by a standard spectrum model, inspired by the von Kármán model. The same spectrum model can be used in both directions because of the assumption of homogeneous turbulence. For example, we have for the along-wind turbulence:

$$\frac{nS_{uu}}{\sigma_u^2} = \frac{A_{k,u}f_u}{1 + B_{k,u}f_u^{\delta_{k,u}}} \quad (5)$$

In the previous equation, $A_{k,u}$, $B_{k,u}$ and $\delta_{k,u}$ are constant parameters, which can be found by nonlinear fitting. The frequency n is normalized to the dimensionless quantity as $f_u = nL_{ux}/\bar{U}$, where L_{ux} is the integral length of along-wind turbulence, \bar{U} is the mean flow speed. In the case of the along-wind turbulence the fitted model, normalized with respect to the variance of the turbulence (σ_u^2), is plotted as a dashed line in Fig. 6(a) and compared against the experimental curve. The same process can be repeated to derive the PSD of the cross-wind turbulence S_{vv} ; the comparison of the normalized spectra is illustrated in Fig. 6(b).

3.3. Wind tunnel test procedure

The CAARC building loads were evaluated for eleven different mean wind directions, $\alpha \in \{0^\circ, 5^\circ, 10^\circ, 15^\circ, 30^\circ, 45^\circ, 60^\circ, 75^\circ, 80^\circ, 85^\circ, 90^\circ\}$. The incremental changes of angle α are smaller around 0° and 90° , where the aerodynamic coefficients change more drastically (Simiu and Scanlan, 1996).

For each wind direction, the CAARC model was tested at seven distinct mean flow speeds, $5 \text{ m/s} < \bar{U} < 11 \text{ m/s}$. At each wind speed, the HFFB testing duration is 600 s; the time series of the base forces and moments are subsequently divided into 20 non-overlapping sub-intervals of 30-s duration. For each 30-s sub-interval, the intermediate 20-s duration portion is extracted and only retained for further analysis. The initial and last parts (5 s) are discarded to ensure independence among the sub-intervals. Each 20-s sub-interval is treated as an independent realization of the random base force or moment process; it is equivalent to approximately a 10-min duration at full scale for this building in consideration of the basic geometric and dynamic similarity characteristics.

4. Modeling of generalized wind force spectra (along-wind force, cross-wind force and torque)

4.1. Preliminary investigation: static aerodynamic load coefficients

The mean wind loads, experimentally measured, are expressed by the three following equations as a function of mean flow speed \bar{U} and density ρ :

$$F_D(\alpha) = \frac{1}{2} C_D(\alpha) \rho \bar{U}^2 D h \quad (6a)$$

$$F_L(\alpha) = \frac{1}{2} C_L(\alpha) \rho \bar{U}^2 D h \quad (6b)$$

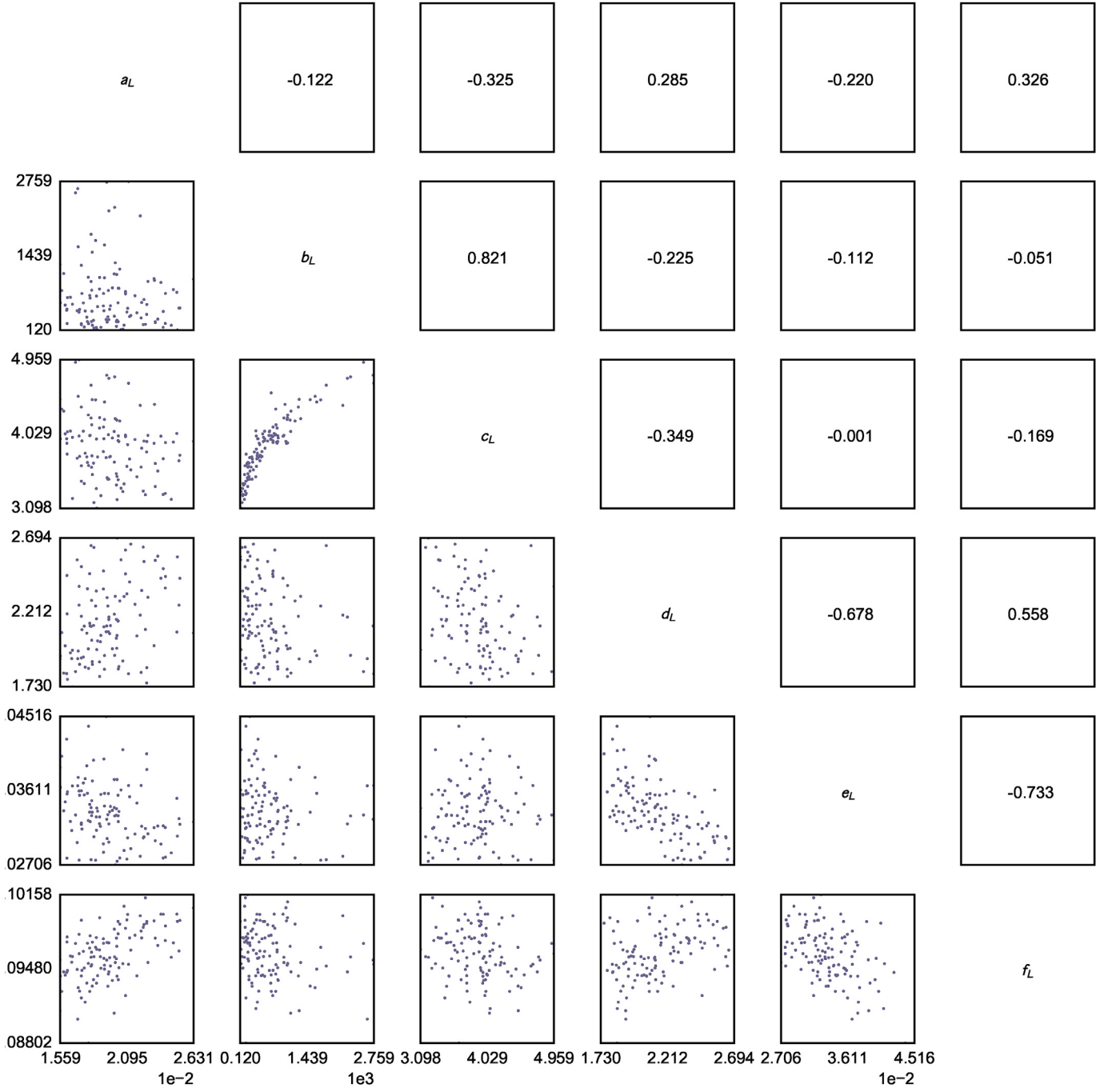


Fig. 17. Coefficients of correlation among the parameters of the cross-wind force PSD model curve in Eq. (10) for the CAARC building model.

$$F_M(\alpha) = \frac{1}{2} C_M(\alpha) \rho \bar{U}^2 D^2 h \quad (6c)$$

In the previous equations, C_D is the drag coefficient, C_L is lift coefficient and C_M is torque coefficient; they depend on the flow incidence angle (α).

The three static wind force coefficients C_D , C_L and C_M obtained from the test result in NEU's wind tunnel are plotted in Fig. 7 as a function of the wind direction α . There are 20×7 data points for each wind direction.

The Reynolds number was variable between 20 000 and 44 000 in the tests. For bluff cylinder with sharp edges, aerodynamic force coefficients can be usually considered insensitive to wind speed. Therefore all three aerodynamic force coefficients at various wind speeds and for the same wind direction should be comparable and may be plotted together (Simiu

and Scanlan, 1996). Even though clear dependency on the wind speed was not exhibited in the experiments, clear variability is visible in Fig. 7, even using the same building model and testing equipment. This phenomenon is attributed to the effects of testing variability and random experimental error. This results directly confirms the merits of this study and necessity for further investigation.

It is also convenient to derive a mathematical model to examine the relationship between each of the three aerodynamic force coefficients C_D , C_L , C_M and the mean wind direction α . A Fourier-series expansion with six parameters, as described in Eq. (7) below with $i = \{D, L, M\}$ and α expressed in degrees, is used to fit the test results from Fig. 7.

$$C_i = a_0 + a_1 \cos(w\alpha) + b_1 \sin(w\alpha) + a_2 \cos(2w\alpha) + b_2 \sin(2w\alpha) \quad (7)$$

The curve fitting results are also presented in each panel of Fig. 7 for

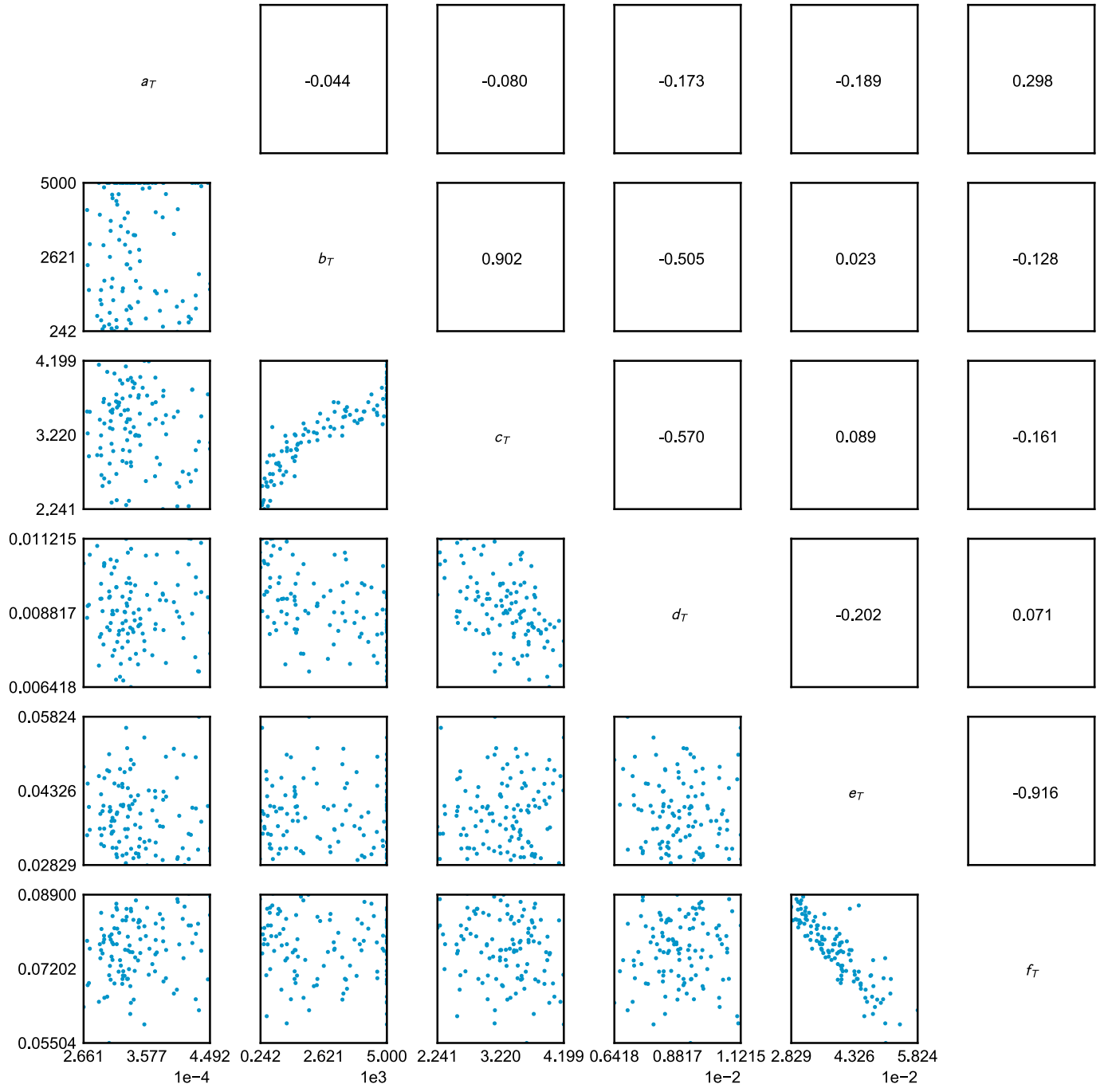


Fig. 18. Correlation among the coefficients of the torque PSD model curve in Eq. (11) for the CAARC building model.

each static coefficient; the values of the parameters in Eq. (7) are summarized in Table 1. The fitted formula can provide a continuous function for any wind direction between 0° and 90°. Moreover, the derivative with respect to α of this equation can be used for the estimation of aerodynamic damping and aerodynamic stiffness properties. Even though the variability of static aerodynamic force coefficients is not the primary study objective, it is important to examine this aspect before moving to the central part of this research, i.e., a direct method to evaluate the PSD of the generalized wind force from the wind tunnel HFFB data.

4.2. Modeling of the generalized wind force spectra: mathematical formulation

In the analysis of the dynamic response of tall buildings, it is

convenient to consider a modal superposition approach, i.e., by integrating the wind loading effects along the building height to obtain a generalized modal force. For example, the along-wind generalized force spectra for the lateral bending mode with shape $\Phi_x(z)$ is normally evaluated using Eq. (1). Truncation of the modal expansion to the fundamental lateral modes (along-wind, cross-wind and torsional) is usually considered adequate for the purposes of dynamic response analysis.

When the structural fundamental modal shape is linear along the height h , $\Phi_x(z) = z/h$, the modal force PSD (e.g., the along-wind modal force $S_{Q_x Q_x}(n)$) of the full scale structure can be directly related to the corresponding base bending moment $S_{M_x M_x}(n)$ measured by an HFFB sensor on a building model as follows [e.g., (Holmes, 1987)]:

$$S_{Q_x Q_x}(n) = \frac{S_{M_x M_x}(n)}{h^2} \quad (8)$$

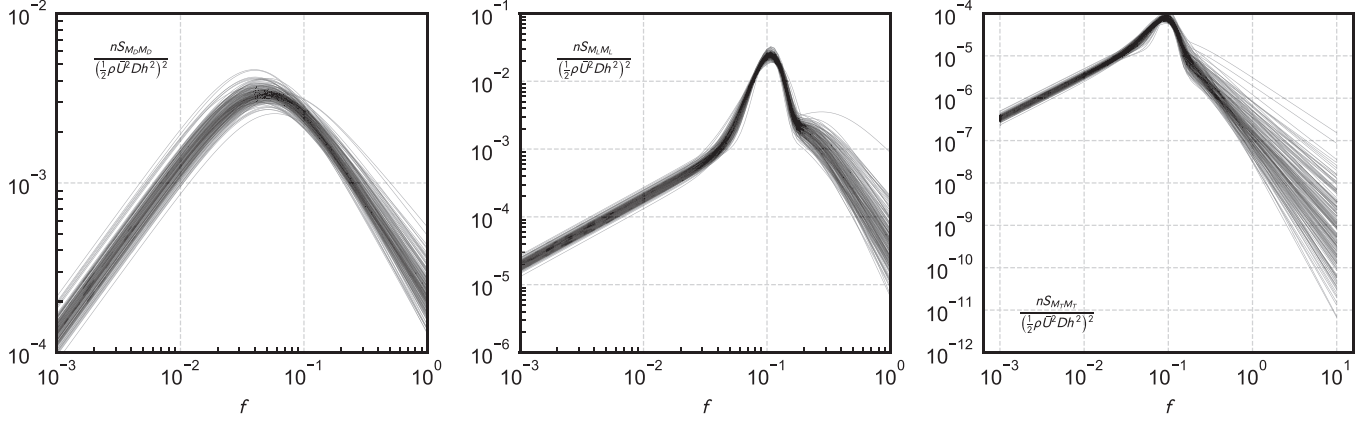


Fig. 19. Synthetically-reconstructed PSD curves: along-wind bending moment, cross-wind bending moment and torque of the CAARC building model for mean wind direction $\alpha = 0^\circ$.

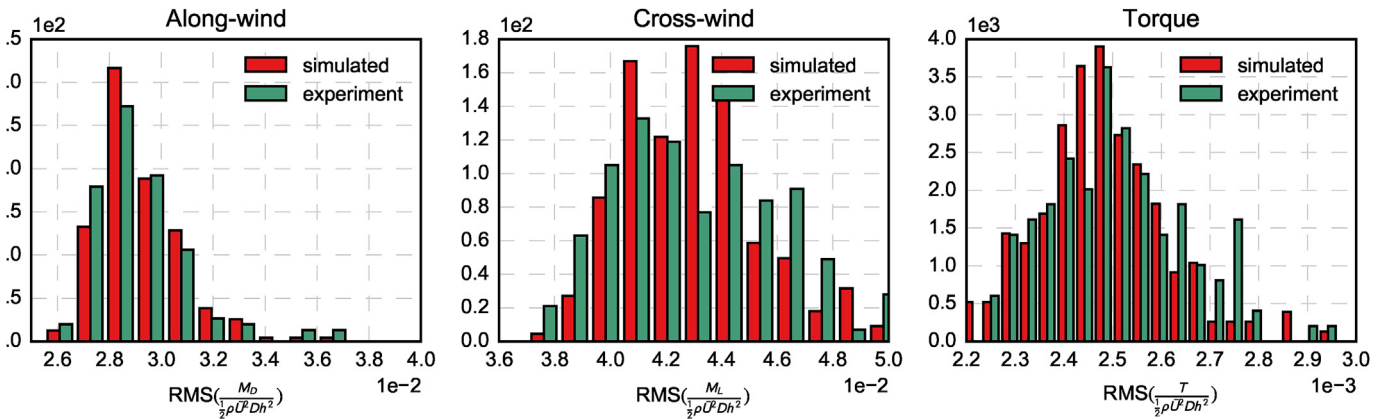


Fig. 20. Synthetically-reconstructed vs. experimental results: comparison among the normalized variances of the along-wind bending moment, cross-wind bending moment and torque for mean wind direction $\alpha = 0^\circ$.

The quantity $S_{M_x M_x}(n)$ is the PSD of the time series of the base bending moment, measured by the HFFB. This technique is widely adopted by wind engineering practitioners [e.g., Reinhold and Kareem (1986); Tschanz and Davenport (1983); Chen and Kareem (2005b); Bernardini et al. (2012)]. Similar expressions are provided for cross-wind generalized force (i.e., HFFB base bending moment). In the case of the torque, the correspondence between measurements and generalized force is not as direct as with the bending moments, especially for non-ideal mode shapes; a review of this aspect may be found, for example, in Tse et al. (2009a).

The quantity $S_{M_x M_x}(n)$ is usually directly evaluated from the experiments on a case-by-case situation and found empirically. Very few studies have attempted to propose a general expression for the quantity $S_{M_x M_x}(n)$ after observing that the shape of the function $S_{M_x M_x}(n)$ may possibly be postulated “a-priori”. One example may be found in the study by Liang et al. (2002); the authors propose a rational-function approximation of the PSD function by using polynomials of various degree in an attempt to fit the empirical shape of the HFFB measurements. Instead of utilizing a set of trial-and-error functions to fit the PSD curve, this paper proposes an approach that considers basic physical principles to postulate a model equation for the PSD function in the frequency domain. The clear advantage is that the proposed formulation preserves the connection with turbulence loading and the theoretical spectra, such as Eq. (5), in both low-frequency and inertial ranges. Even though the test case exclusively considers the CAARC benchmark building as the example, the model equation is general and can possibly be adapted to a wide variety of buildings. In addition, the formulation can also include variability in the experimental loading and enables error and uncertainty quantification.

Since the base bending moment in the along-wind direction is mostly caused by turbulence (buffeting), the corresponding PSD function $S_{M_D M_D}(n) = S_{M_x M_x}(n)$, by considering a structural vibration mode only, can be expressed as:

$$\frac{nS_{M_D M_D}}{\left(\frac{1}{2}\rho\bar{U}^2 D h^2\right)^2} = \frac{a_D f}{1 + b_D f^{c_D}} \quad (9)$$

where the frequency is normalized to dimensionless form $f = nD/\bar{U}$; a_D , b_D and c_D are parameters that can be determined from the experimental base bending moment spectra. Fig. 8 is an example (one realization), using Eq. (9) that fits the along-wind base empirical bending moment when the mean wind speed is $\bar{U} = 9.79$ m/s and wind direction is $\alpha = 0$. Local variations and differences between the experimental spectrum and the fitted curve are noticeable; these differences are expected (locally) and depend on several factors: selection of the fitting algorithm, selection of the number of Fourier points by the Welch's method, length of the record and resolution of the empirical spectrum, etc. Variations are not physically compatible with any spectrum model and, therefore, can possibly be attributed to experimental variability (i.e. later incorporated with the error analysis). The model used to describe the along-wind force was derived from the model of the turbulence spectrum, since the wind force is dominated by the buffeting effect. The use of a different spectrum model (for both turbulence and along-wind force) may have produced a different result. In any case, the spectrum model that was employed adequately describes the main features of the wind force.

For the bending moment and the generalized force in the cross-wind direction, the spectra usually depend on both incoming turbulence and wake excitation (vortex shedding). Therefore, in the previous model

equation the vortex shedding effects should also be included. Due to the periodic nature of vortex shedding in both turbulent and non-turbulent environments, it has been suggested (Vickery and Clark, 1972; Simiu and Scanlan, 1996) that these effects can adequately be modeled using a Gaussian-like model in the frequency domain. As vortex shedding and buffeting can be treated as two nearly-independent phenomena [e.g., (Vickery and Clark, 1972; Simiu and Scanlan, 1996; Piccardo and Solari, 2000)] the fitting equation for the HFFB base moment in the cross-wind direction ($S_{M_L M_L}$) can separately account for the two excitation sources to obtain:

$$\frac{nS_{M_L M_L}(n)}{\left(\frac{1}{2}\rho\bar{U}^2Dh^2\right)^2} = \frac{a_L f}{1 + b_L f^{cl}} + d_L f^2 \exp\left[-\left(\frac{f - e_L}{f_L}\right)^2\right] \quad (10)$$

Similarly, the building's base torque is influenced by both buffeting and wake excitation; consequently, the fitting equation has two terms i.e.:

$$\frac{nS_{TT}(n)}{\left(\frac{1}{2}\rho\bar{U}^2Dh^2\right)^2} = \frac{a_T f}{1 + b_T f^{cr}} + d_T f^2 \exp\left[-\left(\frac{f - e_T}{f_T}\right)^2\right] \quad (11)$$

It should be noted that in most studies [e.g., (Kareem, 1985)], the building base torque is normalized to $\frac{1}{2}\rho\bar{U}^2D^2h$. In this study, the base torque in Eq. (11) is normalized to $\frac{1}{2}\rho\bar{U}^2Dh^2$ rather than $\frac{1}{2}\rho\bar{U}^2D^2h$ to preserve consistency with the normalization employed for along-wind forces and cross-wind base moments and, consequently, generalized forces. Finally, since both cross-wind force and torque are affected by vortex shedding, the parameters e_L and e_T , which locate the peak, should be the same. In the present context and for the purposes of the regression analysis, they were initially assumed as different in Eqs.(10)–(11) and even though they coincide (apart from obvious instrumental resolution).

Figs. 9 and 10 present two examples (two realizations) of the cross-wind bending base moment spectra and base torque, and compare the experimental data points against the model equations.

It must be noted that the cross-spectra between generalized wind forces should be considered. Generally, the correlation between the along-wind force and the cross-wind force and the correlation between the along-wind force and the torsional moment are negligible (Islam et al., 1992). However, the cross-spectral density function between the generalized cross-wind force and the torsional moment may not be negligible. For example, it has been suggested (Kareem, 1985) that the normalized co-spectrum between cross-wind and torsional generalized loads can be assumed equal to 0.6 for prismatic-like buildings, independently of reduced frequency. In this study, cross-spectra were not considered but should possibly be included in future studies.

5. Parameter uncertainty and wind tunnel load variability analysis

As stated earlier, the main purpose of this paper is the exploration of experimental variability and random errors in the evaluation of the generalized wind load PSD. A total of 140 realizations of the HFFB base moments were examined at seven different wind speeds \bar{U} and for each wind direction α .

Fig. 11(a) illustrates the PSD curves of the along-wind base bending moment, measured in the wind tunnel. Each curve is the result of one wind tunnel measurement, derived from the method described in Section 4.2. The horizontal axis is the reduced frequency $f = nD/\bar{U}$; the vertical axis is the normalized PSD of the along-wind base bending moment. The presence of a cluster in the curves suggests that the shape of the PSD base bending moment is similar for the given building model and wind direction. The PSD curves for this direction and other directions exhibit a consistent trend in the results; this consistency suggests that the experimental setup is appropriate for the measurement of the base forces. However, some variability due to random imperfections in the measurements, sensor and digital data communication, is also visible. The

variability does not show a clear dependency on direction or frequency, suggesting that the scatter in the data is likely not a systematic error but a random effect of the laboratory experimental conditions. The cross-wind base bending moment and base torque exhibit similar trends in Fig. 11(b) and (c). The experimental PSD curves show a larger dispersion (standard deviation) at high reduced frequencies ($f > 0.3$ approximately) in comparison with low frequencies in all the three panels of the figure. It is believed that this effect is partially associated with the signal post-processing, which employs the method described in Cui and Caracoglia (2016) to eliminate a spurious resonance effect due to a non-rigid connection detail between the model and the HFFB.

Figs. 12 and 13 illustrate the realizations of the experimental PSD curves along with their variability for other wind directions, respectively for along-wind and cross-wind base bending moments and base torque.

The shapes of the cross-wind and torque PSD curves are significantly influenced by the mean wind direction from Figs. 12 and 13. For the cross-wind PSD curves, the vortex-shedding effects are important when the wind direction is close to $\alpha = 0^\circ$ with a clear peak around the Strouhal frequency; on the contrary the relevance of the wake excitation reduces as the mean wind direction increases. For the wind direction $\alpha = 15^\circ$, the vortex shedding peak has disappeared and the wake excitation contribution to the cross-wind PSD is almost zero. The same trend is visible for the torque PSD; when the wind direction is $\alpha = 10^\circ$, the effect of vortex shedding is insignificant. However, when the mean wind direction $\alpha = 85^\circ$ or $\alpha = 90^\circ$, the vortex shedding peak becomes visible again and important. The bandwidth of the vortex-shedding peaks is in general much broader at $\alpha = 90^\circ$ (wake flow impingement or reattachment due to longer after-body) compared to the wind direction $\alpha = 0^\circ$.

Examination of Figs. 11–13 confirms that the shape of the PSD curves, at a given mean wind direction, is similar but variability (i.e., experimental error) is also present. Therefore, it is plausible to study this error by considering random variations in the coefficients of the model curves in Eqs. (9)–(11). Fig. 14 presents the empirical histograms of the parameters, found from Eqs. (9)–(11) by repeating the fitting for each realization of the PSD curve at $\alpha = 0^\circ$. The fitting results in Fig. 14 were subsequently examined by maximum likelihood estimation method to identify the probability distribution of each parameter. The Gamma probability distribution is a good fit for b_L , b_C and b_T whereas the lognormal distribution is adequate for all the other parameters. In order to verify the adequacy of the distribution models, supplementary statistical analysis was carried out. The results of the goodness-of-fit statistical tests for the identified parameters are illustrated in Fig. 15 for the CAARC building model at $\alpha = 0^\circ$. The hypothesis tests assume that b_D , b_L and b_T follow a Gamma distribution model whereas the remaining parameters are log-normally distributed. In Fig. 15 the p values are presented and compared against the confidence level of 0.05.

For other wind directions, the empirical histograms of the parameters and their corresponding random distribution are similar to the ones found for wind direction $\alpha = 0^\circ$; figures and details are omitted for the sake of conciseness.

6. Monte-Carlo-based reconstruction of base bending moment PSD model equations

In this section, a more detailed and quantitative analysis of the variability in the experimental results of the CAARC building's base bending moments, and Eqs. (9)–(11) is described. Moreover, the randomness in the parameters of the model equations [Eqs. (9)–(11)] is investigated. Since the ultimate goal of this research is the propagation of uncertainty and prediction of structural response variability [i.e., fragility; (Cui and Caracoglia, 2015)], a Monte-Carlo-based method was proposed to synthetically generate a statistically consistent random sample of the generalized loading spectra, which may later be used in conjunction with the approach described in Cui and Caracoglia (2015). If a suitable set of random parameters is randomly generated, accounting for actual experimental variability in the wind tunnel and considering

marginal distributions and correlation, a population of generalized-force PSD curves can be digitally synthesized.

Additionally, the correlations among the parameters need to be carefully analyzed. When the mean wind direction is $\alpha = 0^\circ$, the correlation among the a_D , b_D and c_D in Eq. (9) is presented in Fig. 16 as an example.

The values of a_D , b_D and c_D were found from the PSD curves in Fig. 11(a). The upper-right panels in Fig. 16 present the correlation coefficients between any two parameters in Eq. (9), while the lower-left panels of Fig. 16 display the empirical scatter diagrams between any two parameters. The examination of Fig. 16 confirms that the correlation among the parameters in Eq. (9) is non-negligible and must be carefully considered in the Monte-Carlo simulations.

The correlation coefficients among the parameters for the formula coefficients of cross-wind base bending moment in Eq. (10) and torque in Eq. (11), when the wind direction angle is $\alpha = 0^\circ$, are displayed in Figs. 17 and 18 respectively.

In the reconstruction of the PSD curves, the parameters must be randomly generated (concurrently) in accordance with their marginal distribution characteristics as well as their mutual correlations. In this paper, the Copula method (Nelsen, 2009) was used to reconstruct the random parameters with appropriate probability distributions and correlation. First, a “seed” of correlated uniform random numbers were generated by using a Gaussian Copula. Subsequently, the uniform random numbers were converted to the target parameters satisfying the corresponding cumulative density function of each random parameter with either Gamma or log-normal distribution (Haas, 1999).

The model equation parameters, found using the Copula method, can therefore be used to form a synthetic population of generalized wind force PSD functions at a given wind direction. Fig. 19 illustrates an example of Monte-Carlo-based synthetic generation of along-wind, cross-wind and torque PSD functions for wind direction $\alpha = 0^\circ$.

In order to verify the adequacy of the synthetic wind force PSD reconstruction *vis-à-vis* the experimental curves, the normalized RMS (root mean square) values of the base bending moments found numerically were compared against the experimental values of the RMS. The normalized RMS of the wind forces are computed from the integration of the spectra:

$$\text{RMS}(i) = \sqrt{\int_0^{\infty} s_{ii}(f) df} \quad (12)$$

in which the index $i = \{D,L,T\}$ is used to designate the normalized generalized force; the s_{ii} is the PSD of the normalized forces defined in accordance with Eqs. (9)–(11). Fig. 20 illustrates the comparison of the empirical histograms of RMS(i) for the CAARC building model when the mean wind direction is $\alpha = 0^\circ$; the histograms are estimated by collecting all experimental data samples and the synthetically-reconstructed PSD results. The simulations have the same sample size as the experiments.

Fig. 20 suggests that the empirical distribution of the variances is similar to the one of the simulated data, in the case of all three normalized forces. This remark confirms the effectiveness of the proposed reconstruction method from another view point. Since the comparisons for other wind directions are similar, the figures are omitted.

Verification of robustness was carried out by two-sample Kolmogorov-Smirnov hypothesis test. This test compares two data samples and evaluates whether the samples are related to the same distribution. The two samples that were compared are the experimentally derived RMS values of the generalized base forces and torque and the synthetically-generated ones at various mean wind directions α . In essence, the test analyzes the empirical distribution histograms presented in Fig. 20 for angle $\alpha = 0^\circ$. At $\alpha = 0^\circ$ the p values are 0.33, 0.10 and 0.11 respectively for along-wind and cross-wind forces and torque, indicating that the test is positive at a significance level of 0.05. For other α the tests are generally positive for along-wind and cross-wind forces, whereas some doubts are raised for selected wind directions in the case of the

generalized torque. Therefore, further verification of robustness may be considered.

It must be noted that comparison of each empirical parameter (a_D , b_D , etc.) with the corresponding synthetically-generated values is not feasible. Since experimental data are in the time domain whereas the parameters of the model are evaluated in the frequency domain, a direct transformation or inverse transformation from/to Fourier domain may induce an undesirable error, for example associated with numerical truncation. For this reason, the comparisons based on the RMS results in Fig. 20, the goodness-of-fit tests in Fig. 15 and the two-sample tests described above were used as indicators of robustness. In any case, alternative methods for validation should be considered; these studies are beyond the scope of this work but may be examined in the future.

7. Conclusions

This paper presented the results of an experimentally-based investigation on generalized wind loads for tall buildings at different mean wind directions. The benchmark tall building, used in the wind tunnel tests, is the CAARC standard building.

The experiments, conducted in a small-scale wind tunnel under homogeneous-turbulence flow, acquired several time histories of the along-wind, cross-wind and torque base forces. The study proposed and implemented a series of model equations [Eqs. (9)–(11)], based on basic physical principles, to describe the power spectral density of the corresponding generalized wind load on the prototype structure for multi-directional winds. The model equations drastically simplify the derivation of the wind force formulas, the identification of which may become very complex and cumbersome when several wind directions need to be studied. In addition, the examination of the experimental PSD curves [Figs. 11–13] suggests that, for each mean wind direction, the PSD curves are qualitatively similar even though non-negligible variability was noted. The differences, attributed to random experimental errors, can be suitably represented by statistical analysis of the parameters in Eqs. (9)–(11). The study also demonstrates that the concept of model equation enables the generation of a statistically-consistent set of synthetic PSD functions by Monte-Carlo sampling and Copula method, reproducing the experimental variability. The inter-dependence among the parameters of the model curves should be considered. The comparison between the synthetic PSD curves and the experimental results indicates that simulations results are consistent with experiments in the case of the CAARC building and suggests that this approach could promisingly be used to investigate uncertainty propagation in building aerodynamics. Even though the experiments were carried out in homogeneous turbulence flow, similar results are anticipated in the case of boundary layer wind turbulence. Observations from an earlier study (Cui and Caracoglia, 2016) confirmed that the overall shape of the PSD curves is similar to the reference literature results, obtained with boundary layer open terrain exposure (Saunders and Melbourne, 1975); this remark translates into a potential applicability of the model equations to a wider range of cases.

Acknowledgments

Messrs. Kurt Braun and Michael MacNeil of NEU's Department of Civil and Environmental Engineering are gratefully acknowledged for construction and assembly of the experimental setup and for technical assistance during the execution of the tests. Messrs. David Abati and Darren Vokes of NEU's Carpentry Department are gratefully acknowledged for the design, fabrication and assembly of the test chamber. Professor Jerome F. Hajjar and the NEU's Department of Civil and Environmental Engineering are gratefully acknowledged for the collaboration with sensor equipment. Finally, the authors would like to thank Professor Hanchen Huang and the NEU's Department of Mechanical and Industrial Engineering for the shared use of wind tunnel facility.

This material is based upon work supported in part by the National

Science Foundation (NSF) of the United States under CAREER Award CMMI-0844977 in 2009–2014. The partial support of NSF Award CMMI-1434880 is also acknowledged. Any opinions, findings and conclusions or recommendations are those of the authors and do not necessarily reflect the views of either the NSF or any other sponsor.

References

- Bernardini, E., Spence, S.M., Gioffrè, M., 2012. Effects of the aerodynamic uncertainties in HFFB loading schemes on the response of tall buildings with coupled dynamic modes. *Eng. Struct.* 42, 329–341.
- Bernardini, E., Spence, S.M., Kwon, D.-K., Kareem, A., 2014. Performance-based design of high-rise buildings for occupant comfort. *J. Struct. Eng.* 04014244.
- Boogs, D., Peterka, J., 1989. Aerodynamic model tests of tall buildings. *J. Eng. Mech.* 115 (3), 618–635.
- Caracoglia, L., 2014. A stochastic model for examining along-wind loading uncertainty and intervention costs due to wind-induced damage on tall buildings. *Eng. Struct.* 78, 121–132.
- Caracoglia, L., Sangree, R.H., Jones, N.P., Schafer, B.W., 2008. Interpretation of full-scale strain data from wind pressures on a low-rise structure. *J. Wind Eng. Ind. Aerodyn.* 96 (12), 2363–2382.
- Chen, X., Kareem, A., 2005a. Coupled dynamic analysis and equivalent static wind loads on buildings with three-dimensional modes. *J. Struct. Eng. (ASCE)* 131 (7), 1071–1082.
- Chen, X., Kareem, A., 2005b. Dynamic wind effects on buildings with 3D coupled modes: application of high frequency force balance measurements. *J. Eng. Mech. (ASCE)* 131 (11), 1115–1125.
- Chen, X., Kareem, A., 2005c. Validity of wind load distribution based on high frequency force balance measurements. *J. Struct. Eng.* 131 (6), 984–987.
- Chock, G., Boogs, D., Peterka, J., 1998. A wind and hurricane design framework for multi-hazard performance-based engineering of high-rise buildings. *Struct. Eng. World Wide* T139–3.
- Corrigan, A., Camelli, F.F., Löchner, R., Wallin, J., 2011. Running unstructured grid-based CFD solvers on modern graphics hardware. *Int. J. Numer. Methods Fluids* 66 (2), 221–229.
- Cui, W., Caracoglia, L., 2015. Simulation and analysis of intervention costs due to wind-induced damage on tall buildings. *Eng. Struct.* 87 (0), 183–197.
- Cui, W., Caracoglia, L., 2016. Physics-based method for the removal of spurious resonant frequencies in High-Frequency Force Balance tests. *J. Struct. Eng. ASCE* 142 (2), 04015129.
- Davenport, A.G., 1961. A Statistical Approach to the Treatment of Wind Loading on Tall Masts and Suspension Bridges. Ph.D. Dissertation. University of Bristol, United Kingdom.
- Davenport, A.G., 1971. The response of six building shapes to turbulent wind. *Philos. Trans. Royal Soc. Lond. Ser. A, Math. Phys. Sci.* 269 (1199), 385–394.
- Davenport, A.G., 1988. The response of supertall buildings to wind. In: Second Century of the Skyscraper. Springer, pp. 705–725.
- Davenport, A.G., Tschanz, T., 1981. The response of tall buildings to wind. In: Proceedings of the Fourth US National Conference of Wind Engineering. Seattle, Washington, USA.
- Dyrbye, C., Hansen, S.O., 1997. Wind Loads on Structures, first ed. John Wiley & Sons, New Jersey, USA.
- Ellingwood, B., Rosowsky, D., Li, Y., Kim, J., 2004. Fragility assessment of light-frame wood construction subjected to wind and earthquake hazards. *J. Struct. Eng.* 130 (12), 1921–1930.
- Ellingwood, B., Tekie, P., 1999. Wind load statistics for probability-based structural design. *J. Struct. Eng.* 125 (4), 453–463.
- Elshaer, A., Aboshosha, H., Bitsuamlak, G., Damatty, A.E., Dagnew, A., 2016. LES evaluation of wind-induced responses for an isolated and a surrounded tall building. *Eng. Struct.* 115, 179–195.
- Haas, C.N., 1999. On modeling correlated random variables in risk assessment. *Risk Anal.* 19 (6), 1205–1214.
- Holmes, J., 1987. Mode shape corrections for dynamic response to wind. *Eng. Struct.* 9 (3), 210–212.
- Huang, M., Chan, C., Lou, W., 2012. Optimal performance-based design of wind sensitive tall buildings considering uncertainties. *Comput. Struct.* 98–99, 7–16.
- Huang, S., Li, Q., Xu, S., 2007. Numerical evaluation of wind effects on a tall steel building by CFD. *J. Constr. Steel Res.* 63 (5), 612–627.
- Islam, M.S., Ellingwood, B., Corotis, R.B., 1992. Wind-induced response of structurally asymmetric high-rise buildings. *J. Struct. Eng. (ASCE)* 118 (1), 207–222.
- Isyumov, N., 2012. Alan G. Davenport's mark on wind engineering. *J. Wind Eng. Ind. Aerodyn.* 104, 12–24.
- Jain, A., Srinivasan, M., Hart, G.C., 2001. Performance based design extreme wind loads on tall building. *Struct. Des. Tall Build.* 10 (1), 9–26.
- Kareem, A., 1982. Across wind response of buildings. *J. Struct. Div.* 108 (4), 869–887.
- Kareem, A., 1985. Lateral-torsional motion of tall buildings. *J. Struct. Eng. ASCE* 111 (11), 2497–2496.
- Kareem, A., Cermak, J., 1978. Wind tunnel simulation of wind-structure interactions. In: International Instrumentation Symposium, 24 th, Albuquerque, N. Mex, Proceedings. Part 2, vol. 1.
- Lee, S., Bobby, S., Spence, S., Tovar, A., Kareem, A., 2012. Shape and topology sculpting of tall buildings under aerodynamic loads. In: 20th Analysis and Computation Specialty Conference. ASCE, pp. 323–334.
- Liang, S., Liu, S., Li, Q., Zhang, L., Gu, M., 2002. Mathematical model of crosswind dynamic loads on rectangular tall buildings. *J. Wind Eng. Ind. Aerodyn.* 90 (12–15), 1757–1770.
- Melbourne, W.H., 1980. Comparison of measurements on the CAARC standard tall building model in simulated model wind flows. *J. Wind Eng. Ind. Aerodyn.* 6 (1), 73–88.
- Nelsen, R.B., 2009. An Introduction to Copulas, second ed. Springer, New York, USA.
- Piccardo, G., Solari, G., 1998a. Closed form prediction of 3-D wind-excited response of slender structures. *J. Wind Eng. Ind. Aerodyn.* 74, 697–708.
- Piccardo, G., Solari, G., 1998b. Generalized equivalent spectrum technique. *Wind Struct.* 1 (2), 161–174.
- Piccardo, G., Solari, G., 2000. 3D wind-excited response of slender structures: closed-form solution. *J. Struct. Eng. (ASCE)* 126 (8), 936–943.
- Pozzuoli, C., Bartoli, G., Peil, U., Clobes, M., 2013. Serviceability wind risk assessment of tall buildings including aeroelastic effects. *J. Wind Eng. Ind. Aerodyn.* 123 (Part B), 325–338.
- Reinhold, T.A., Kareem, A., 1986. Wind loads and building response predictions using force balance techniques. In: Dynamic Response of Structures. ASCE, pp. 390–397.
- Saunders, J., Melbourne, W., 1975. Tall rectangular building response to cross-wind excitation. In: Proc. 4th Int. Conf. On Wind Effects on Buildings and Structures. Cambridge University Press, London, pp. 369–380.
- Seo, D.W., Caracoglia, L., 2012. Statistical buffeting response of flexible bridges influenced by errors in aeroelastic loading estimation. *J. Wind Eng. Ind. Aerodyn.* 104, 129–140.
- Simiu, E., Scanlan, R.H., 1996. Wind Effects on Structures fundamentals and applications to design, third ed. John Wiley & Sons, New Jersey, USA.
- Smith, M.A., Caracoglia, L., 2011. A Monte Carlo based method for the dynamic “fragility analysis” of tall buildings under turbulent wind loading. *Eng. Struct.* 33 (2), 410–420.
- Spence, S.M., Kareem, A., 2014. Performance-based design and optimization of uncertain wind-excited dynamic building systems. *Eng. Struct.* 78, 133–144.
- Tschanz, T., Davenport, A., 1983. The base balance technique for the determination of dynamic wind loads. *J. Wind Eng. Ind. Aerodyn.* 13 (1–3), 429–439.
- Tse, K., Hitchcock, P., Kwok, K., 2009a. Mode shape linearization for HFBB analysis of wind-excited complex tall buildings. *Eng. Struct.* 31 (2), 675–685.
- Tse, K., Hitchcock, P., Kwok, K., Thepmongkorn, S., Chan, C., 2009b. Economic perspectives of aerodynamic treatments of square tall buildings. *J. Wind Eng. Ind. Aerodyn.* 97 (9–10), 455–467.
- van de Lindt, J., Dao, T., 2009. Performance-based wind engineering for wood-frame buildings. *J. Struct. Eng.* 135 (2), 169–177.
- Vickery, B.J., Clark, A.W., 1972. Lift or across-wind response to tapered stacks. *J. Struct. Div.* 98 (1), 1–20.
- Zhou, Y., Kareem, A., Gu, M., 2002. Mode shape corrections for wind load effects. *J. Eng. Mech. (ASCE)* 128 (1), 15–23.